A Numerically Efficient Method for Predicting the Scattering Characteristics of Complex Moving Targets

A Numerically Efficient Method for Predicting the Scattering Characteristics of Complex Moving Targets

Dihia Sidi Ahmed, Paola Russo *Member, IEEE*, Graziano Cerri, Laetitia Thirion Lefèvre, Régis Guinvarc'h, Giovanni Manfredi

***Abstract*—This paper presents a new computational approach that allows rapid analysis of the Electro-Magnetic Scattering characteristics (EMS) of static or moving complex radar targets. The scattering features of the object are represented through a generalized scattering matrix H, whose elements can be measured or computed using conventional numerical techniques, e.g., CST software in the proposed case, and considering prescribed sampled directions. A cardinal series then is adopted to reconstruct the complete scattering pattern by suitably extending the approach to calculate the target's scattering matrix for any incidence wave and any observation point. The number of finite samples, that is, the dimension of the scattering matrix depends only on the maximum dimension of the target. A PEC sphere and a PEC three-dimensional (3D) complex object have been analyzed in detail. Precise, fast, and stable sampling algorithms have been applied to these targets in the static case and in motion. In particular, the field scattered by the moving objects is then used to carry out the Micro-Doppler analysis of the object radar signature.**

***Index Terms*—Electromagnetic modeling, Moving Targets, Scattered Field**

I. Introduction

Target detection and recognition is an intensely investigated topic in radar research. Previous research focused on modeling and evaluating the scattering characteristics (SC) of static targets. The parameter considered for this evaluation is the Radar Cross Section (RCS). The RCS has been analyzed and recovered with different techniques: various models exist for canonical and metallic targets [1] [2], or more complex objects like the human body [3] [4]. For electrically large objects, high-frequency methods are used [5], such as physical optics (PO), geometrical theory of diffraction (GTD) [6], and uniform theory of diffraction (UTD) [7]; for resonant objects, full-wave approaches such as Method of Moment (MOM) [8], are required to characterize 3D scattering [9]. Recently, researchers have shifted their interest to detecting and recognizing moving objects. In this context, the RCS, a scalar quantity, is not adequate enough to recover their signature, because an accurate evaluation of the scattered signal phase changes is required. Moving parts in the object and its movement can create different RCS. Therefore a good knowledge about Micro-Doppler or Doppler signature , and SC of moving objects is essential for their recognition or analysis [10]. In literature, many papers deal with moving targets, adopting essentially experimental techniques. Moreover, the classification of different events is usually done in conjunction with the deep learning approach. For example, in [11], the analysis is applied for the recognition of falling events, whereas in [12] and [13], it is applied for discriminating different human activities. In [14], the authors realized a system that recognizes a moving pedestrian for application in an autonomous driving car.

A more challenging application is the detection of Unmanned Aerial vehicles (UAV), particularly small ones. The surge in popularity of these types of aerial devices increased the interest in their characterization and classification [15] [16] [17], and made detecting them crucial [18]. The difficulty in recognizing such a target is due to its weak radar signature [19] [20]. Also, in this case, many papers propose using machine learning to improve detection. It is well known that this approach requires huge labeled datasets to generate robust models. Researchers generate the data using indoor or outdoor measurements [21], but these methods suffer from a lack of labeled datasets. Modeling can solve some of these problems; making the scene as realistic as possible can compensate for this lack. It facilitates the micro-Doppler analysis by providing information on the effect of the radar response on the receiving signal, allowing us to study the degradation of the detection performance in the presence of obstacles. In general, the physics-based model allows a better understanding of the interactions between radar wave and the target and, therefore, which parts of the target exhibit the most significant signature [22]. There are a few publications on modeling the radar response of moving targets. In [23], the authors simulate the Doppler response of a target with rotating parts, using a ray technique. In [24] and [25], modeling of the scattered response of human bodies was carried out. However, no electromagnetic calculation was performed so that the physical complexity was avoided. Concerning electromagnetic models, analytical tools

D. Sidi Ahmed is with SONDRA, CentraleSupélec, Université Paris-Saclay, F-91190 Gif-sur-Yvette, France, and the Department of Information Engineering, Università Politecnica delle Marche, Ancona, 60131, Italy (email: dihia.sidi-ahmed@centralesupelec.fr)

P. Russo is with the Department of Information Engineering, Università Politecnica delle Marche, Ancona, 60131, Italy (email: p.russo@staff.univpm.it)

G. Cerri is with the Department of Information Engineering, Università Politecnica delle Marche, Ancona, 60131, Italy (email: g.cerri@staff.univpm.it)

L. Thirion-Lefèvre is with SONDRA, CentraleSupélec, Université Paris-Saclay, F-91190 Gif-sur-Yvette, France (email: Laetitia.Thirion@centralesupelec.fr)

R. Guinvarc'h is with SONDRA, CentraleSupélec, Université Paris-Saclay, F-91190 Gif-sur-Yvette, France (email: Regis.Guinvarch@centralesupelec.fr)

G. Manfredi is with SONDRA, CentraleSupélec, Université Paris-Saclay, F-91190 Gif-sur-Yvette, France (email: giovanni.manfredi@centralesupelec.fr)

can be very flexible, but they are hardly applicable to complex geometries; software tools are very sophisticated [26] and allow the scattering evaluation of complex isolated objects, but they can be extremely heavy when evaluating the movement and interaction with other objects since it is necessary to repeat several times the entire electromagnetic computation of the target's SC under different illuminations. Therefore, it is necessary to have a tool that can provide fast, efficient calculations of SC of a target, both static or in movement.

This paper proposes a simple tool for modeling the SC of an object, that can be used for a fast evaluation of its SC also when moving at non-relativistic velocity. The method is based on the evaluation of a generalized version of the scattering matrix, that is usually applied to microwave junctions, characterized by a **finite** number of input/output ports. On the contrary, in our case, the system is open, so it is characterized by an **infinite** number of input (incident field direction) /output (scattering directions) ports. In order to create a finite matrix, the ports are sampled so that a finite number of elements can be handled. A subsequent interpolation technique, based on cardinal series, is applied every time it is necessary to know the SC of the target for whatever impinging and scattering direction of the field. This matrix, named H, replaces the RCS parameter in our method, giving us not only the amplitude but also the phase information of the scattered field. The method proposed is fast and accurate. The strong computation and time-consuming effort are related to the creation of the library of H-matrix for a wide range of possible targets, but once the matrix of a specific target is ready, it can be used for whatever situation of impinging wave angles and scattering angles. The reconstruction method is very fast. The proposed technique is also flexible, because the generalized scattering matrix can be obtained in different ways: measurements or numerical tools. Moreover, it can be used to integrate models that account for the presence of different environments (urban, forest, etc.) or to create a large dataset for machine learning classification, removing the limitations of the measurement approach.

The reliability and accuracy of the method are tested by applying it to the evaluation of the field scattered from two different targets: a metallic sphere and a metallic object of complex geometry. The same objects, moving in different scenarios, are studied to show how the method can be efficiently applied to reconstruct the radar signature of moving objects, and how these data can be usefully processed for the Micro-Doppler analysis.

This paper is structured as follows: Section II is a description of the formulation of the problem. Section III is a step-by-step description of the formulation of our model. Section IV presents a validation of the proposed method by comparing it with the results derived by using the simulation software (CST) and with measurements; finally, the conclusion is given in Section V.

II. Formulation of the Problem

This work describes a new approach to the analysis of the standard bistatic radar configuration, where a transmitting antenna Tx illuminates an object that moves at velocity v. The field scattered by the target is evaluated at the receiving antenna location Rx. Fig. 1 shows the problem's geometry, (R_T,Θ,Φ) and (R_R,θ, ϕ) represent the positions of the transmitting and receiving antennas, respectively, with respect to a spherical coordinate system centered on the target. Throughout the paper, the angular coordinates (Θ,Φ), written in uppercase Greek letters, will indicate the direction of the incident wave, whereas the angular coordinates (θ, ϕ), written in lowercase Greek letters, will indicate the direction of the scattered wave.

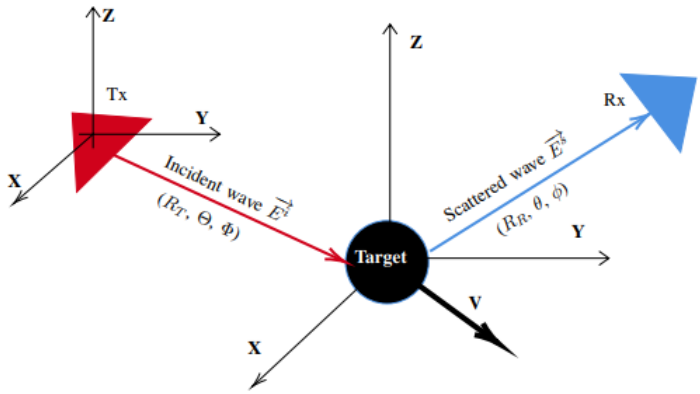

Fig. 1: The geometry of the scenario: the Tx antenna radiates a moving object, and the scattered field is evaluated at the receiving antenna Rx.

As it moves, the target changes its position relative both to the transmitting and the receiving antenna, and an accurate representation of the field at the receiving point requires a continuous re-computation of the scattered field. This aspect generally represents a very cumbersome burden, from a computational point of view. Therefore a numerically efficient technique is necessary to characterize the scattered field along the entire path of the target.

The basic idea is to represent the field $\overrightarrow{E^s}$ (R_R,θ, ϕ), scattered by the target in the observation point due to an incident field $\overrightarrow{E^i}$ (R_T,Θ, Φ) as written in Equation (1):

$$\overrightarrow{E^s}(R_R,\theta,\phi) = H(\Theta,\Phi,\theta,\phi) \times \overrightarrow{E^i}(R_T,\Theta,\Phi)\frac{e^{-j\beta R_R}}{R_R} \quad (1)$$

where β is the propagation constant, and H is a [3 × 3] matrix defined as:

$$H = \begin{bmatrix} h_x^x & h_y^x & h_z^x \\ h_x^y & h_y^y & h_z^y \\ h_x^z & h_y^z & h_z^z \end{bmatrix} \quad (2)$$

with all the components of H depending on Θ, Φ, θ, and ϕ.

Each element $h_{x_q}^{x_p}(\Theta,\Phi,\theta,\phi)$, of the matrix represents the x_p component $(p = 1,2,3)$ of the far-field scattered by the object in direction (θ,ϕ), calculated at the distance a, normalized to the x_q component $(q = 1,2,3)$ of the incident field impinging from direction (Θ,Φ), where $(x_1 = x, x_2 = y, x_3 = z)$.

The field is evaluated at a proper reference distance a chosen in the far-field region of the object, having a role similar to the reference planes at the ports of a microwave network.

Therefore, each element of the matrix H can be evaluated as:

$$h_{x_q}^{x_p}(\Theta,\Phi,\theta,\phi) = ae^{j\beta a}\frac{E_{x_p}^{s}(\theta,\phi)}{E_{x_q}^{i}(\Theta,\Phi)} \tag{3}$$

It is important to note that, by its definition, matrix $H(\Theta,\Phi,\theta,\phi)$ depends on object characteristics only. A fast and accurate method to evaluate Equation (2) for any direction of arrival (Θ,Φ) of the impinging field and any scattering direction (θ,ϕ) is developed and described in the next section. It is worth briefly mentioning the notation used throughout the paper. For practical purposes, essentially because the object is thought to be inside a complex 3D space, all field components are represented in Cartesian coordinates. The target position and the receiving point location are referred to a fixed Cartesian system (O, X, Y, Z) centered on the transmitting antenna. As the object experiences an incident field and re-radiates a scattered field, it is convenient to adopt a second reference system (O', x, y, z), centered on the moving target, which also defines the spherical system used to evaluate the direction (Θ,Φ) of the incident field and (θ,ϕ) of the scattered field. Standard coordinate transformation equations allow us to pass easily from one system to another.

III. Generation of the matrix H

The angular coordinates that define the direction of arrival of the impinging field and the scattering direction of the receiving point are a function of the object position; therefore, to describe the electromagnetic signature of a moving object, the matrix H in (2) has to be computed for each point of the target trajectory. Even if the matrix H can be evaluated using analytical, numerical, or experimental methods, its continuous re-computation makes the approach extremely cumbersome and difficult. In order to speed up the procedure without losing accuracy, the method described below has been developed. It is based on the evaluation of the scattered field in a discrete number of properly selected directions and on the use of an interpolation technique to generalize the approach.

The procedure of generation of the matrix H and of the subsequent interpolation technique will be presented in two steps: 1) the generation of the matrix for a specific impinging wave direction. 2) the generation of the matrix for a generic impinging wave direction.

A. Reconstruction of the scattered field for one impinging wave on the target

In order to outline the method, we first refer to the simple situation described in Fig. 2, which depicts the scenario for the generation of the scattered field values, in the case of only one particular direction of arrival of the incident wave, characterized by the elevation angle Θ_i and azimuth angle Φ_{ij}.

The same figure also shows some possible scattering directions, and the reference surface of radius a in the far-field region of the object. In particular, a number of specific discrete scattering directions, characterized by the elevation angle θ_m, $0 \le m \le M$ and azimuth angle ϕ_{mn}, $0 \le n \le N$, are properly selected.

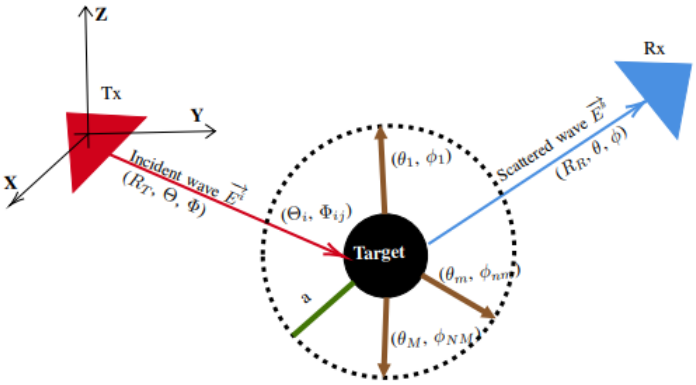

Fig. 2: Geometry of the problem: the scattering object is surrounded by the sphere of radius a used for sampling the scattered field.

After this simple preliminary setting, the electromagnetic scattering problem is solved. In our case, we used the CST tool [26], extensively validated in literature and by the authors themselves, adopting the following procedure:

- the object geometry and materials are implemented in CST;
- the electromagnetic solver simulates a plane wave impinging from direction (Θ_i,Φ_{ij});
- the scattered field is evaluated in all points (a,θ_m,ϕ_{mn}) with $0 \le m \le M$; $0 \le n \le N$ and stored.

This simple procedure provides a matrix **H** (written in bold font) of order greater than the order of matrix H (written in italic font), and whose structure is represented in Fig. 3, where, for convenience, it is conceived as a 2D sheet. It is worth noting that each element of the matrix **H** is itself a [3 × 3] matrix H defined in Equation (2), whose elements are given by:

$$h_{x_q}^{x_p}(\Theta_i,\Phi_{ij},\theta_m,\phi_{mn}) = ae^{j\beta a}\frac{E_{x_p}^{s}(\theta_m,\phi_{mn})}{E_{x_q}^{i}(\Theta_i,\Phi_{ij})} \tag{4}$$

with $0 \le m \le M$ and $0 \le n \le N$.

For Equation (4), the same notation used for Equation (3) has been adopted. The matrix term in Equation (4) represents the component x_p of the scattered field in direction (θ_m,ϕ_{mn}), normalized to the component x_q of the incident field, impinging from (Θ_i,Φ_{ij}). Its value does not depend on the far-field distance a. The scattered field must be calculated in the object's far-field region; otherwise, a near-field to far-field transformation would be necessary for evaluating the scattered field in a general situation.

If the direction (θ,ϕ) of the observation point of the scattered field is different from any selected direction (θ_m,ϕ_{mn}), a proper interpolation technique is adopted. Therefore, the problem is the evaluation of the terms $h_{x_q}^{x_p}(\Theta_i,\Phi_{ij},\theta,\phi)$ in Equation (2), using an algorithm that is as fast and accurate as possible, from knowledge of the matrix **H**, whose elements are given by Equation (4). The adopted solution is based on

the method developed in [27], where the field representation through a cardinal series is used. The cardinal series proposed in [27] is based on spherical coordinates, and a proper sampling procedure is suggested. Details of the sampling and interpolation procedure adopted in our case are reported in the Appendix of this paper.

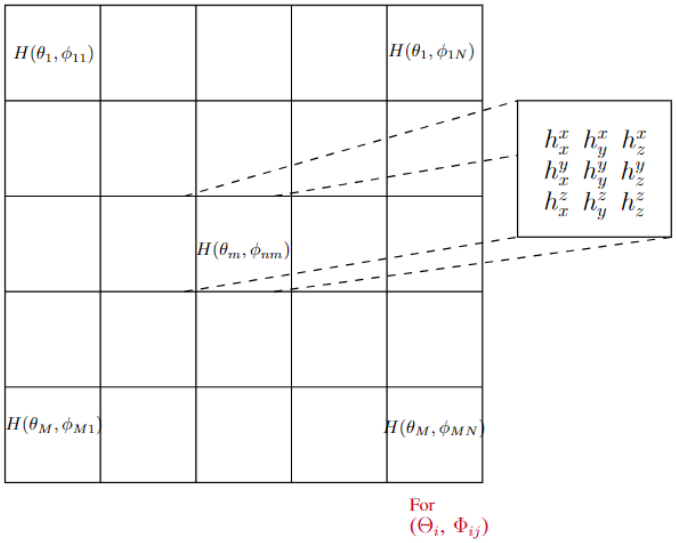

Fig. 3: Structure of the matrix **H**, for the storage of the scattered field sampled in selected directions due to a plane wave impinging from direction (Θ_i, Φ_{ij}).

B. Reconstruction of the scattered field for general impinging wave on the target

In a general situation, especially for the case of a moving object:

- neither direction (Θ, Φ) of the impinging wave nor direction (θ, ϕ) of the observation point of the scattered field are a priori known,
- they are generally different from the directions selected for creating, **H** matrix and moreover
- they change continuously.

Therefore, the problem now is the evaluation of the general terms $h_{x_q}^{x_p}(\theta, \phi, \Theta, \Phi)$.
To solve this problem, the idea of sampling the direction of the field, expressed in III-A, is once again applied, but this time to the incident field direction. This is a generalization of the method proposed in [27] that deals only with the scattering field. It is necessary to create all the matrices **H** generated by plane waves impinging from many different selected incident directions (Θ_i, Φ_{ij}), $0 \leq i \leq I$; $0 \leq j \leq J$. For the sake of simplicity, we choose $I = M$ and $J = N$ so that the integer numbers that define the selected incident directions are the same as those for scattering directions [28], in this way also the selected directions of wave arrival and scattering coincide. This procedure provides an even higher-order matrix $\mathbb{H}(\theta_m, \Phi_{mn}, \Theta_i, \Phi_{ij})$ that can be conceived as the 3D structure shown in Fig. 4 made up of many layers, one layer for each

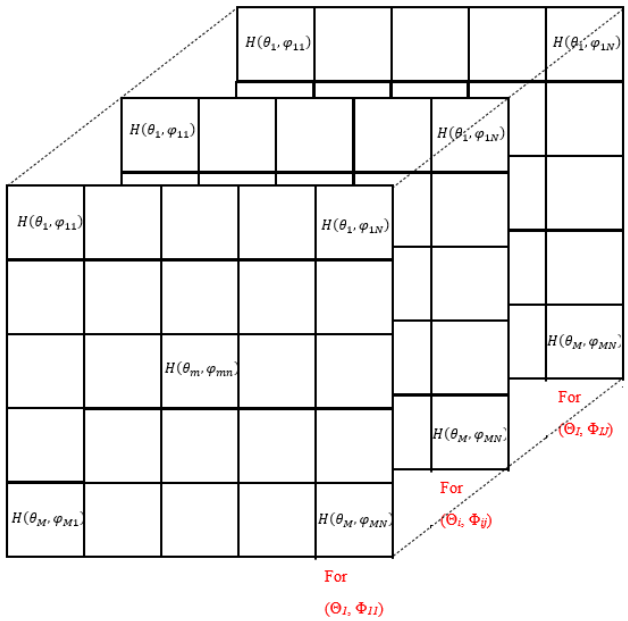

Fig. 4: Structure of the 3D matrix $\mathbb{H}(\theta_m, \phi_{mn}, \Theta_i, \Phi_{ij})$, for the storage of the scattered field sampled in selected directions (θ_m, ϕ_{mn}), $0 \leq m \leq M$ and $0 \leq n \leq N$, due to plane waves impinging from selected directions (Θ_i, Φ_{ij}), $0 \leq i \leq I$; $0 \leq j \leq J$.

direction of the impinging wave. The matrix elements are once again defined by Equation (4).

It is worth noting that in the implementation of the method:

1) the matrix $\mathbb{H}$ elements are evaluated only once, off-line, and at the beginning of the procedure;
2) any electromagnetic approach (analytic, numerical, experimental) can be used to fill the matrix $\mathbb{H}$;
3) the matrix $\mathbb{H}$ completely characterizes the 3D scattering of the object, taking into account its shape, dimensions, and materials.

Knowledge of the matrix $\mathbb{H}$ allows us to analyze all possible situations from the trivial case where the direction of arrival of the impinging wave (Θ_i, Φ_{ij}) and scattering direction (θ_m, ϕ_{mn}) coincides with one of those selected, up to the most general one, where the direction of the arrival of the impinging wave (Θ, Φ) and scattering direction (θ, ϕ) do not coincides with any sampling directions. The first case is the simplest situation because the [3 × 3] matrix H to be used in Equation (1) is the element $H(\theta_m, \phi_{mn})$ for (Θ_i, Φ_{ij}) of the 3D matrix $\mathbb{H}$, and no further calculation is required. For the general case, in order to have the correct matrix H to be used in Equation (1), the interpolation technique through the cardinal series is applied twice, the first time over the scattering directions and the second time over the impinging directions. The sequential application of the interpolation technique provides Equation (5), which is a very simple and efficient form to be implemented with an algorithm.

$$h_{x_q}^{x_p}(\Theta,\Phi,\theta,\phi) = \sum_{i=-M}^{M}\sum_{j=-N}^{N}\sum_{m=-M}^{M}\sum_{n=-N}^{N} h_{x_q}^{x_p}(\Theta_i,\Phi_{ij},\theta_m,\phi_{mn}) \cdot \frac{\operatorname{sinc}\left((2N+1)\frac{\phi-\phi_{mn}}{2}\right)}{\operatorname{sinc}\left(\frac{\phi-\phi_{mn}}{2}\right)} \frac{\operatorname{sinc}\left((2M+1)\frac{\theta-\theta_m}{2}\right)}{\operatorname{sinc}\left(\frac{\theta-\theta_m}{2}\right)} \frac{\operatorname{sinc}\left((2N+1)\frac{\Phi-\Phi_{ij}}{2}\right)}{\operatorname{sinc}\left(\frac{\Phi-\Phi_{mn}}{2}\right)} \frac{\operatorname{sinc}\left((2M+1)\frac{\Theta-\Theta_i}{2}\right)}{\operatorname{sinc}\left(\frac{\Theta-\Theta_i}{2}\right)} \quad (5)$$

where the sampling angles are provided in the appendix.

Equation (5) represents the normalized field scattered by the object in a generic direction (θ,ϕ), for the generic direction (Θ,Φ) of the impinging wave. The amplitudes of the series terms are the elements of the matrix $\mathbb{H}$, evaluated in Equation (4). It can be noted that the 3D matrix $\mathbb{H}$ is used as a whole in the most general situation, whereas for the other simpler cases (reported in the appendix) only sub matrices are considered. Summarizing, the electromagnetic signature of a moving object, at a non relativistic velocity , can be obtained according to the following procedure:

1) the 3D matrix $\mathbb{H}(\Theta_i,\Phi_{ij},\theta_m,\phi_{mn})$ that characterizes the object is calculated (only once) using the definitions of its elements given in Equation (4);
2) coordinates (θ,ϕ) and (Θ,Φ) are determined from the knowledge of the object position;
3) equation (5) is applied, obtaining the elements of the [3 × 3] matrix $H(\theta,\phi,\Theta,\Phi)$ in Equation (2), to be used in Equation (1) to evaluate the scattered field;
4) changing the object position, the algorithm restarts from step 2 of the procedure.

IV. Results

The accuracy and efficiency of the proposed method were tested by applying the model to two different situations: a static target and a moving one, both in free space. Two targets were considered: a PEC sphere and a complex PEC structure called UFO (Unidentified Flying Object). The first test concerns the reconstruction of the scattered field in the far-field region for both targets, and the second test regards a micro-Doppler analysis. The second test, which analyses the electromagnetic scattering of a moving object, is particularly severe as far as computational efficiency is concerned, because it requires the generation of a great deal of data. In particular, this test highlights the efficiency of the proposed method because, once the 3D matrix $\mathbb{H}$ is known, it is not necessary to repeat its evaluation for every target position, but it is simply necessary to apply Equation (5) for the different directions of the impinging and scattered waves. The first object chosen for numerical tests is a PEC sphere, whose diameter is 20 cm. The second object is the complex PEC structure shown in Fig. 5, whose maximum dimension is 50 cm. It was designed to test

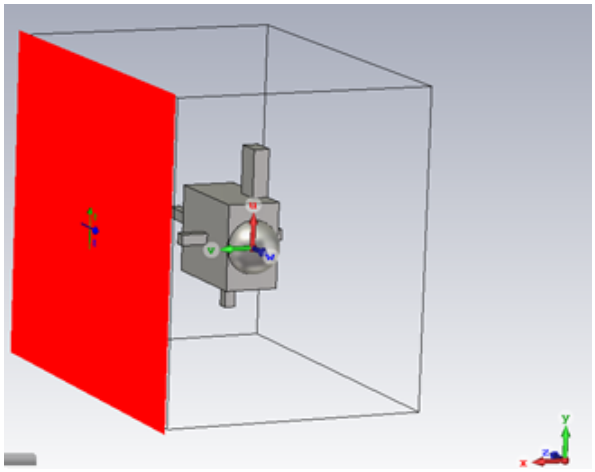

Fig. 5: Geometry of the complex object used to test the method.

and stress the method because it does not exhibit symmetries, and consists of a combination of different shapes with many scattering edges.

An overall error is introduced to quantify the effect of the interpolation technique on the accuracy of the method for the scattered field computation, this overall error is defined as:

$$err = \frac{\sum\left(|E_{ref}-E_{rec}|\right).|E_{ref}|}{\sum|E_{ref}|^2} \quad (6)$$

Where, E_{ref} is the scattered field evaluated with the CST, and is considered the reference field to be compared to E_{rec} that is the scattered field reconstructed with the proposed method. We can observe that the difference between the reference and reconstructed field is weighted with its value in each point: the more intense the field is at a point, the more significant is the error on its evaluation.

A. Scattered field evaluation

The scenario used to test the accuracy of the scattered field evaluation is based on a target illuminated by a plane wave. The procedure is implemented according to the steps described at the end of section III.

An important aspect concerns the number of sampling directions that depends on the spatial bandwidth of the problem (see appendix for reference) that depends on the radius a of the reference sphere used to evaluate the field and on the frequency of the impinging wave. Considering the dimensions of two targets and an impinging wave of frequency $f = 500MHz$, the total number of samples are, respectively, 199 for the sphere and 352 for the second target, if the spatial bandwidth W is evaluated considering the radius a equal to the far-field distance $a = \frac{2d^2}{\lambda}$, with d being the maximum object dimension. These numbers could be considered too large because of the computational effort necessary for the matrix H evaluation according to Equation (5), affecting the method's efficiency. For this reason, many tests were conducted to analyze the possibility of reducing the sampling directions. Good results have been obtained by evaluating the spatial

bandwidth $W = \chi\beta d$, using the maximum dimension of the target instead of the far-field distance. In this way, the number of samples is reduced to 37 for the sphere and 149 for the second target, obtaining a satisfactory trade-off between accuracy and efficiency.. It is worth highlighting that the electric field samples are still evaluated in the far-field region, and the positions of the sampling directions are once again evaluated according to Equations (A.1) and (A.2).

Results obtained for the targets illuminated by an horizontal-polarized plane wave, with incident angles of (Θ = 90°, Φ = 270°) and a frequency of 500 MHz, are shown in Fig. 6 for the sphere and Fig. 7 for the UFO. In particular, the figures show the scattered far-field components evaluated in the $\phi = 0$ plane, at a distance of 1 m from the sphere and 10 m from the UFO, due to an impinging plane wave having an incident field of 1 V/m. The scattered field is evaluated in directions different from the sampling directions. The same figure also shows the same results obtained directly with the CST as a reference: in both cases, the reconstruction of the scattered field is very good. In particular, the error, using Equation (6), is 0.08% for the sphere and 2% for the UFO.

Regarding the computational efficiency of the reconstruction procedure, it depends on the tool that implements the algorithm given in Equation (5). In our case, we use a MATLAB code, obtaining a simulation time less than 10 seconds for the calculation of the Matrix $\mathbf{H}$ of a generic impinging wave, and time simulation lesser than 0.2 seconds for the calculation of the scattering field at a generic point. This method is implemented to automatically calculate the scattered field in the other object positions when it is moving. When compared with CST, 15 seconds are required to calculate the scattered field at one position, without considering the time it takes to manually implement the configuration pertaining to other positions, so we can conclude that our model is efficient in terms of computational time and implementation.

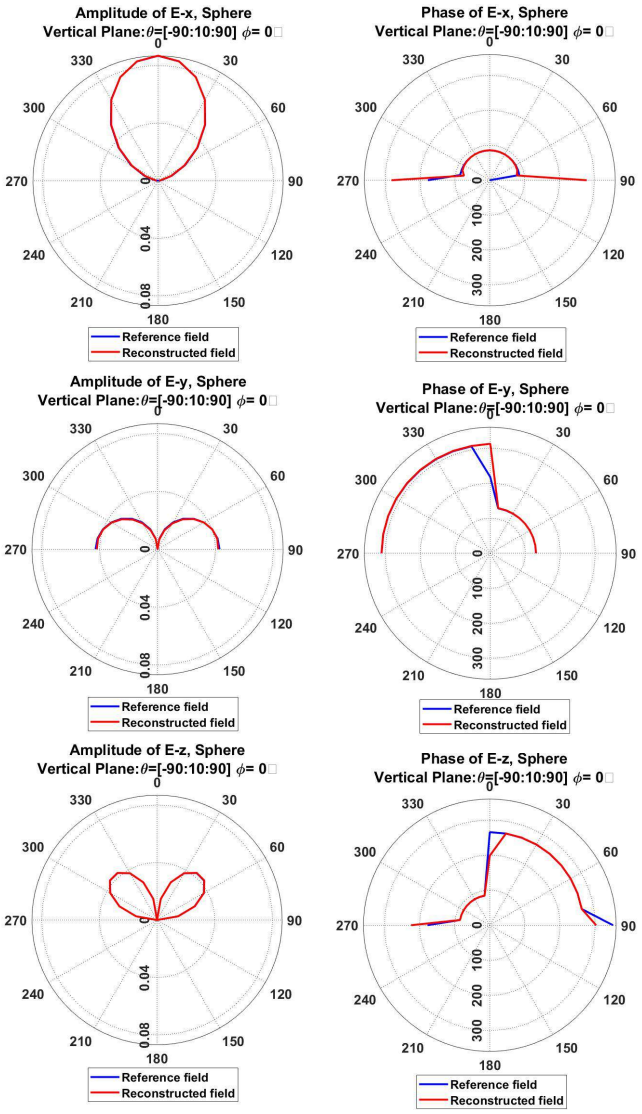

Fig. 6: Reconstruction in the plane $\phi = 0$ of the field scattered by the sphere in both amplitude and phase compared to the reference field calculated using CST.

B. Micro-Doppler analysis

Micro-Doppler analysis can be carried out considering a moving target. As a first simple example, the problem presented in Fig. 8 is considered; the PEC sphere translates along the x-direction from position P1 (-40m, 10m, 0) to position P2 (40m, 10m, 0). The transmitting antenna Tx is supposed to have a gain of 0 dBi and fed with 1w, and positioned in (0, 0, 0); the PEC sphere scattered field is calculated at the fixed receiving antenna located in (0, 20 m, 0). The impinging field has a horizontal polarization. The sphere moves with a velocity of 8 m/s, and to perform the Doppler analysis, its position is sampled every 12.5 ms, corresponding to a displacement of 10 cm between consecutive positions.

To describe the whole path, 801 different positions are analyzed, which implies that Equation (5) must be calculated 801 times. Fig. 9 shows the behavior of the amplitudes and phases of the scattered field components calculated at the receiving point. As expected, the Ex-component is dominant and exhibits a symmetric behavior due to the regular shape of the object and geometric symmetry of the scenario. Instead, the Ez-component is negligible, being more than two orders of magnitude smaller than the Ex-component. Its asymmetric behaviour can be ascribed to the intrinsic approximation of the interpolating technique that has a greater effect on the smaller components. These values were used for the Micro-Doppler analysis of the scenario shown in Fig. 8 and the results are reported in Fig. 10.

The Doppler frequency modulations have been analytically calculated for a working frequency of 500 MHz, according to the Equation (7) of the bistatic Doppler shift [29], defined as follows:

$$F_D = \frac{2||\vec{v}||}{\lambda} \cos\left(\frac{\beta}{2}\right) \cos\delta \tag{7}$$

F_D denotes the target bistatic Doppler frequency for stationary transmitter and receiver, $\vec{v}$ the vector velocity, λ the wavelength, β the bistatic angle, and δ the aspect angle formed between the axis of the bistatic bisector and the axis of the movement, the vector velocity $\vec{v}$ [30] as shown in Fig. 8, in the proposed case, we assume that the sphere will translate along

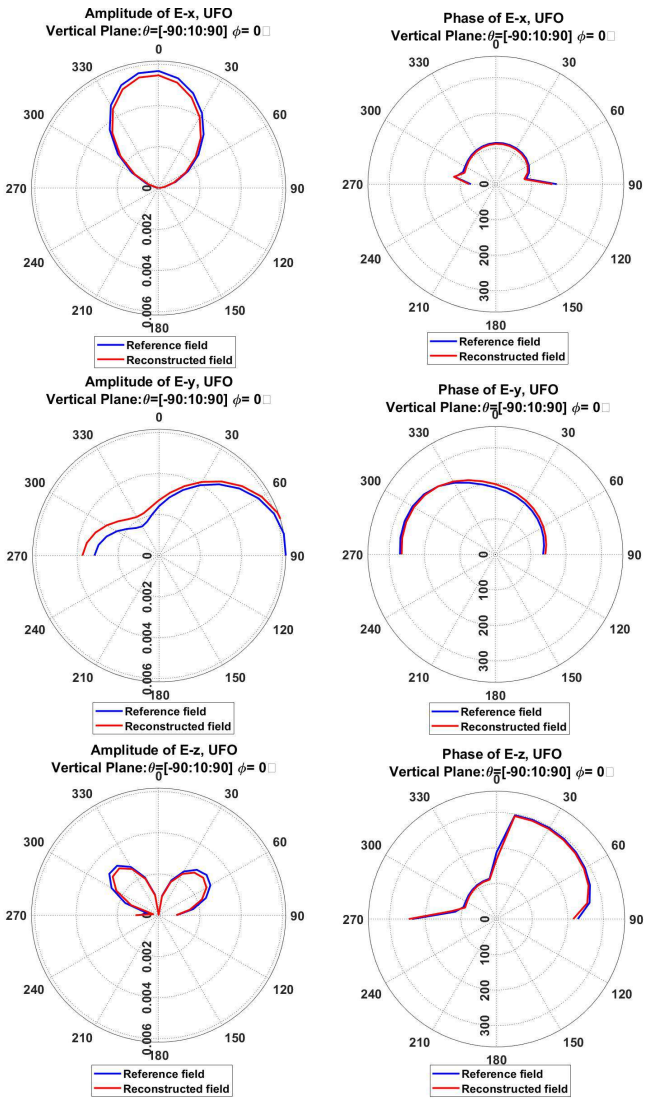

Fig. 7: Reconstruction in the plane $\phi = 0$ of the field scattered by the UFO in both amplitude and phase compared to the reference field calculated using CST.

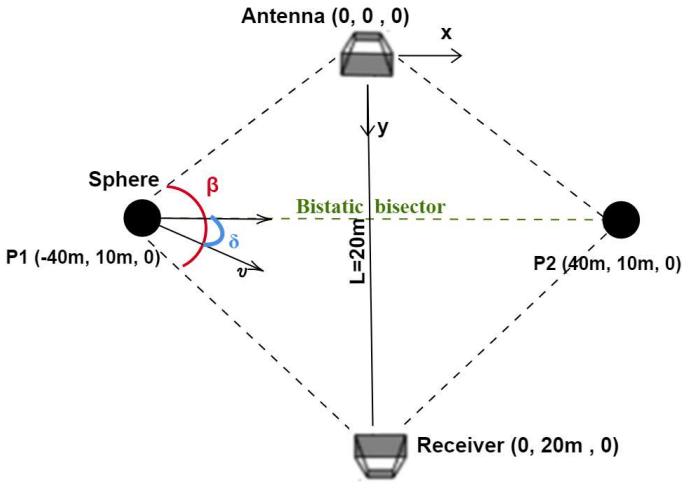

Fig. 8: Set-up of the translation of the PEC sphere along x-axis.

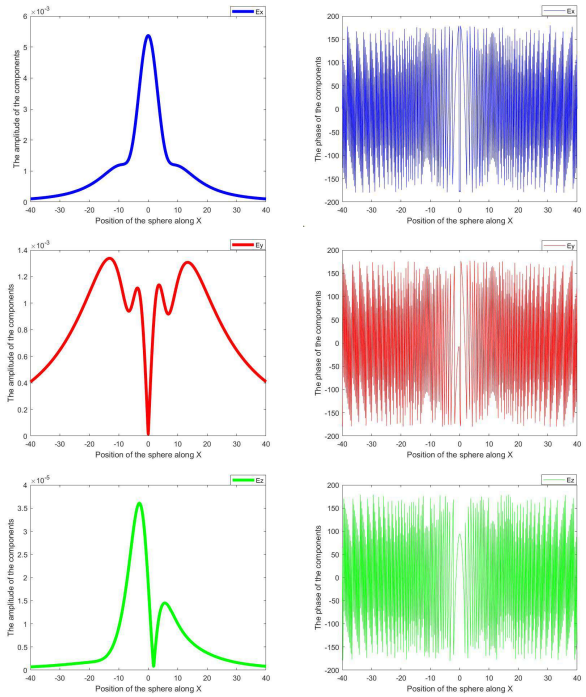

Fig. 9: Amplitudes and phases of the scattered field components Ex, Ey, Ez, at the receiving point calculated for each PEC sphere's position.

the bistatic bisector axis; consequently, the aspect angle $\delta = 0$. The Doppler signature of the moving sphere analyzed at 500 MHz and its prediction is shown in Fig. 10 and manifests the expected behavior: the power is strongly detected when the target is closer to the antennas. When the sphere crosses the line between the antennas, the speed is zero because of the orthogonality between the object direction and the scattering direction. Doppler frequency tends to the correct value when the sphere is far from the antennas, with positive values when the sphere approaches antennas and negative ones when it moves away.

A second, more complex example was considered: the Micro-Doppler analysis of a sphere moving along a curved path. For this case, an experimental validation was performed. It is worth noting that the same 3D matrix $\mathbb{H}$ of a sphere is used in both examples. This is the strongest point of our procedure that makes it possible to analyse any Doppler scenario of the same target without repeating the procedure of evaluating the sampled matrix. Fig. 11 shows the scenario and the path used for the validation of the test. The same scenario was created inside the Antenna Lab of our Department, and the scattering field was measured using a network analyzer. The Doppler analysis results obtained from the experimental data are shown in the top plot, and results obtained with our method are shown in the bottom plot of Fig.12. The harmonic behavior of the velocity component in the x-direction is well reconstructed, as shown by comparing simulation results and measurements. The model also determines the Doppler frequency with completely satisfactory accuracy. The good result of this validation test allows us to consider the proposed

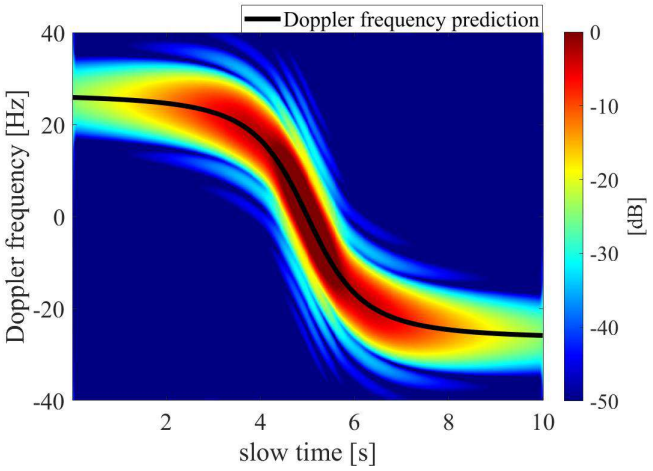

Fig. 10: The Doppler frequency signature of a sphere translating along X axis at 500 MHz: HH polarization, and its Doppler frequency prediction in black curve.

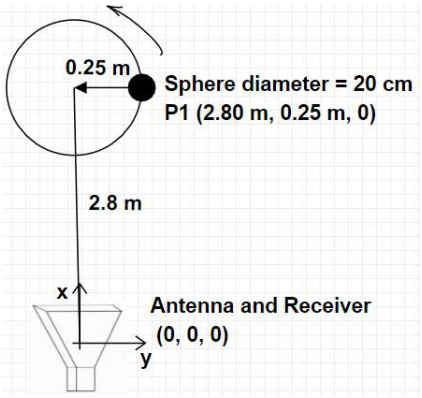

Fig. 11: The simulation and measurement set-up for the curved path of the sphere.

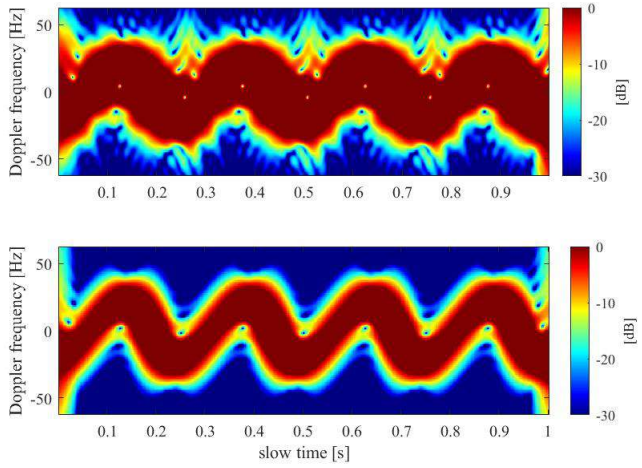

Fig. 12: The Doppler frequency signature of a sphere moving along a curved path and its comparison to measurements.

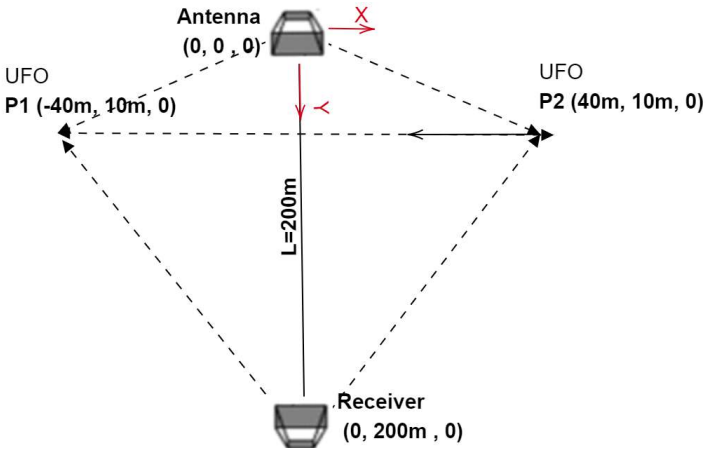

Fig. 13: Set-up of the translation of the PEC UFO along the x-axis.

method as reliable and able to simulate complex scenarios. The amplitude of the component is normalized to its maximum value for both simulation and measurement.

Micro-Doppler analyses are carried out considering the UFO as the moving target, the same configuration of the PEC sphere Micro-Doppler analysis is considered as depicted in Fig. 13, but, the scattered field is calculated at the fixed receiving antenna located in (0, 200 m, 0).

Fig. 14 shows the behavior of the amplitudes and phases of the scattered field components calculated at the receiving point. As expected, the field components are asymmetric, due to the asymmetric geometry of the target, the Ex-component is dominant, and we notice an increase of the amplitude when the object is moving toward the antennas and a decrease when it is moving away from the antennas. The Doppler signature of the moving UFO analyzed at 500 MHz and its prediction is shown in Fig. 15. Two main aspects can be observed in the Doppler frequency signature: the comparison with the bi-static Doppler shift Equation (7) shows the effect of the complexity of the object geometry, since the theoretical Doppler frequency is not the average value of the simulated scenario, as for example, the Doppler signature of the sphere, but it is affected by the target shape. The second aspect concerns the algorithm's numerical efficiency. In the analyzed situation, the receiving point is much further away than in the case of the sphere, but the increased dimension of the scenario doesn't affect the computational time because in the generalized scattering matrix approach, the characterization of the object is performed only once at the beginning of the procedure, so that the computing time for the field evaluation doesn't depend on the scenario dimension.

V. Conclusion

This paper presents an efficient formulation for analyzing the scattering characteristics of static and moving targets. The work aims to develop a method to provide the theoretical electromagnetic signature in a general point of a 3D space of a complex object moving in an electromagnetic field radiated by an antenna. The method is simple in principle

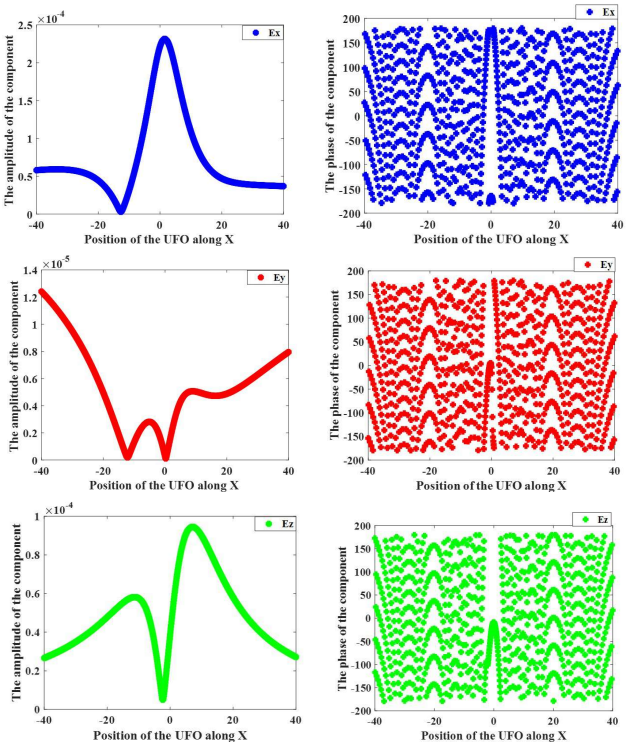

Fig. 14: Amplitudes and phases of the scattered field components Ex, Ey, Ez, at the receiving point calculated for each UFO's position.

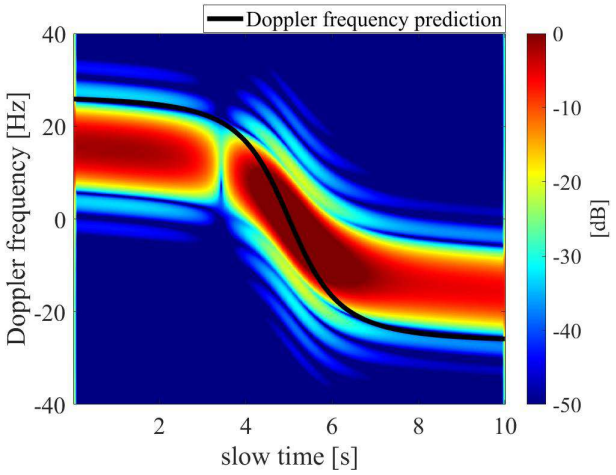

Fig. 15: The Doppler frequency signature of a UFO translating along the x-axis at 500 MHz: HH polarization, and its Doppler frequency prediction in black curve.

and can be easily implemented on a computer. It is based on the object's scattered field knowledge in specific space directions due to plane waves impinging from other specific directions. It is worth noting that this part of the procedure is carried out only once, at the beginning of the analysis, and completely characterizes the object's scattered field accounting for its shape and materials. It can be accomplished using whatever electromagnetic simulation tool. The generalization to any incident and scattering direction is achieved using an interpolating technique based on the cardinal series, suitable for an efficient computer implementation.

The capability of the algorithm to reconstruct the scattered field and its accuracy has been tested for two objects, a metallic sphere and a complex object, comparing their results with those achieved by a full-wave numerical tool, obtaining a good agreement. Other results have concerned the Doppler analysis of moving targets. As the evaluation of the scattered field is required for many points along the object trajectory, the aim was to show the computational efficiency of the method and test the capability of reconstructing the target electromagnetic signature. In this case, some experimental measurements allowed us to validate the numerical simulations. The method's reliability will allow us to approach some realistic scenarios in the near future, such as a drone flying in an urban environment. In fact, the model is self-consistent and can be easily hybridized with other methods, such as PO or ray-tracing, or GTD, to consider, in the mentioned scenario, the effect of the buildings or the ground on the electromagnetic signature of the target.

APPENDIX

This Appendix shows details of the sampling and successive interpolation procedure necessary to obtain the element of the $\mathbb{H}$ matrix. The sampling procedure adopted is based on a uniform distribution of the samples on a spherical surface. For this reason, applying a uniform sampling for the elevation angle (θ_m) it results in a number of samples for the azimuth angles that depends on the elevation angles (ϕ_{mn}).

The maximum number of the samples depends on the spatial bandwidth of the scattering system $W = \chi\beta a$ [27], where a is the radius of the sphere enclosing the scattering system,β is the propagation constant, and χ is the excess bandwidth factor whose value has to be slightly greater than unity (typically 1.2) for an accurate convergence of the interpolation scheme. In particular, the sampling direction considered are

$$\theta_m = \Theta_i = \frac{2\pi m}{2M+1} \tag{A.1}$$

$$\phi_{mn} = \Phi_{ij} = \frac{2\pi n}{2N+1} \tag{A.2}$$

and

$$M = I = \lceil \chi\beta a \rceil \tag{A.3}$$

$$N = J = \lceil \chi\beta a \sin\theta_m \rceil \tag{A.4}$$

It is worth noting that the number of samples is odd and that the range of both angles is $[0 - 2\pi]$. Fig. A.1 shows the distribution of the samples over the sphere, where the samples that have an elevation angle from 0 to π are drawn in black, whereas the samples that have the elevation angles that range from π to 2π are drawn in red. Also, the uniform distribution of the samples can be observed in Fig. A.1.

The elements of matrix H necessary for Equation (1) are reconstructed using the following equations. In particular, we distinguish two simple cases:

- The direction of the arrival of the impinging wave (Θ_i, Φ_{ij}) coincides with one of those selected, but the

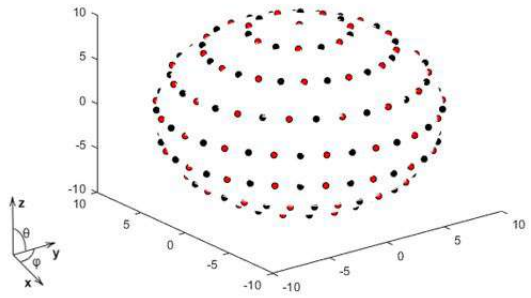

Fig. A.1: Samples distribution on the sphere.

scattering direction (θ, ϕ) is generic. This is the case shown in section III-A and the interpolation technique proposed in [27] is used. We have to enter the layer of the 3D matrix $\mathbb{H}$ characterized by (Θ_i, Φ_{ij}), and use the elements of that layer to calculate the elements of Equation (2).

$$h_{x_q}^{x_p}(\Theta_i, \Phi_{ij}, \theta, \phi) = \sum_{m=-M}^{M} \sum_{n=-N}^{N} h_{x_q}^{x_p}(\Theta_i, \Phi_{ij}, \theta_m, \phi_{mn}) \cdot \frac{\operatorname{sinc}\left((2N+1)\frac{\phi-\phi_{mn}}{2}\right)}{\operatorname{sinc}\left(\frac{\phi-\phi_{mn}}{2}\right)} \frac{\operatorname{sinc}\left((2M+1)\frac{\theta-\theta_m}{2}\right)}{\operatorname{sinc}\left(\frac{\theta-\theta_m}{2}\right)} \tag{A.5}$$

- The direction of arrival of the impinging wave (Θ, Φ) is generic, but the scattering direction (θ_m, ϕ_{mn}) coincides with one of those selected. In this case, an interpolation is also necessary, but for the evaluation of the [3 × 3] matrix H, we have to use the elements $H(\theta_m, \phi_{mn})$ stored in the layers for all impinging waves (Θ_i, Φ_{ij}) $0 \leq i \leq I$; $0 \leq j \leq J$, so that, in this case, the interpolation is performed over all impinging directions.

$$h_{x_q}^{x_p}(\Theta, \Phi, \theta_m, \phi_{mn}) = \sum_{i=-M}^{M} \sum_{j=-N}^{N} h_{x_q}^{x_p}(\Theta_i, \Phi_{ij}, \theta_m, \phi_{mn}) \cdot \frac{\operatorname{sinc}\left((2N+1)\frac{\Phi-\Phi_{ij}}{2}\right)}{\operatorname{sinc}\left(\frac{\Phi-\Phi_{ij}}{2}\right)} \frac{\operatorname{sinc}\left((2M+1)\frac{\Theta-\Theta_i}{2}\right)}{\operatorname{sinc}\left(\frac{\Theta-\Theta_i}{2}\right)} \tag{A.6}$$

REFERENCES

[1] M. B. Heydari, M. Asgari, M. Zolfaghari, and N. Jafari, "Comparison of various full-wave softwares in calculating the RCS of simple objects," *International Journal of Mechatronics, Electrical and Computer Technology (IJMEC)*, vol. 8, pp. 4002–4008, 2018.

[2] P. Besnier, J. Sol, and S. Meric, "Estimating radar cross-section of canonical targets in reverberation chamber," 09 2017, pp. 1–5.

[3] P. Sanchez-Olivares, L. Lozano, Somolinos, and F. Cátedra, "EM modelling of monostatic RCS for different complex targets in the near-field range: Experimental evaluation for traffic applications," *Electronics*, vol. 9, no. 11, 2020. [Online]. Available: https://www.mdpi.com/2079-9292/9/11/1890

[4] G. Manfredi, P. Russo, A. De Leo, and G. Cerri, "Efficient simulation tool to characterize the radar cross section of a pedestrian in near field," *Progress In Electromagnetics Research C*, vol. 100, pp. 145–159, 2020.

[5] D. Bouche, F. Molinet, and R. Mittra, "Asymptotic and hybrid techniques for electromagnetic scattering," *Proceedings of the IEEE*, vol. 81, no. 12, pp. 1658–1684, 1993.

[6] A. Gorji, B. Zakeri, and R. Janalizadeh, "Physical optics analysis for RCS computation of a relatively small complex structure," *Applied Computational Electromagnetics Society Journal*, vol. 29, 03 2014.

[7] M.-J. Algar, L. Lozano, J. Moreno, I. González, and F. Cátedra, "An efficient hybrid technique in RCS predictions of complex targets at high frequencies," *Journal of Computational Physics*, vol. 345, pp. 345–357, 2017.

[8] J. Sidhu, E. Kuster, P. Friederich, and E. Hopkins, "Rcs prediction comparison between physical optics and moment method techniques," in *IEEE Antennas and Propagation Society International Symposium 1997. Digest*, vol. 2, 1997, pp. 1148–1151 vol.2.

[9] F. T. Ulaby and C. Elachi, "Radar polarimetry for geoscience applications," *Geocarto International*, vol. 5, pp. 38–38, 1990.

[10] L. Vignaud, A. Ghaleb, J. le kernec, and J.-M. Nicolas, "Radar high resolution range micro-Doppler analysis of human motions," 11 2009, pp. 1 – 6.

[11] H. Sadreazami, M. Bolic, and S. Rajan, "Contactless fall detection using time-frequency analysis and convolutional neural networks," *IEEE Transactions on Industrial Informatics*, vol. 17, no. 10, pp. 6842–6851, 2021.

[12] U. Saeed, S. Y. Shah, S. A. Shah, J. Ahmad, A. A. Alotaibi, T. Althobaiti, N. Ramzan, A. Alomainy, and Q. H. Abbasi, "Discrete human activity recognition and fall detection by combining FMCW radar data of heterogeneous environments for independent assistive living," *Electronics*, vol. 10, no. 18, 2021. [Online]. Available: https://www.mdpi.com/2079-9292/10/18/2237

[13] Y. Lang, C. Hou, Y. Yang, D. Huang, and Y. He, "Convolutional neural network for human micro-Doppler classification," in *Proc. European Microwave Conference*, 2017.

[14] P. Held, D. Steinhauser, A. Koch, T. Brandmeier, and U. T. Schwarz, "A novel approach for model-based pedestrian tracking using automotive radar," *IEEE Transactions on Intelligent Transportation Systems*, pp. 1–14, 2021.

[15] J. Farlik, M. Kratky, J. Casar, and V. Stary, "Radar cross section and detection of small unmanned aerial vehicles," in *2016 17th International Conference on Mechatronics - Mechatronika (ME)*, 2016, pp. 1–7.

[16] L. To, A. Bati, and D. Hilliard, "Radar cross section measurements of small unmanned air vehicle systems in non-cooperative field environments," in *2009 3rd European Conference on Antennas and Propagation*, 2009, pp. 3637–3641.

[17] C. J. Li and H. Ling, "An investigation on the radar signatures of small consumer drones," *IEEE Antennas and Wireless Propagation Letters*, vol. 16, pp. 649–652, 2017.

[18] D. Sathyamoorthy, "A review of security threats of unmanned aerial vehicles and mitigation steps," *The Journal of Defence and Security*, vol. 6, p. In press, 10 2015.

[19] D. S. Ahmed, L. Thirion-Lefèvre, R. Guinvarc'h, I. Hinostroza, G. Manfredi, P. Russo, and G. Cerri, "Monostatic radar cross section simulation of small unmanned aerial vehicles in UHF band," in *2020 IEEE International Symposium on Antennas and Propagation and North American Radio Science Meeting*, 2020, pp. 1101–1102.

[20] D. De Quevedo, F. I. Urzaiz, J. G. Menoyo, and A. A. López, "Drone detection and RCS measurements with ubiquitous radar," in *2018 International Conference on Radar (RADAR)*, 2018, pp. 1–6.

[21] B. Taha and A. Shoufan, "Machine learning-based drone detection and classification: State-of-the-art in research," *IEEE Access*, vol. 7, pp. 138 669–138 682, 2019.

[22] F. Brigui, L. Thirion-Lefevre, G. Ginolhac, and P. Forster, "New sar algorithm based on orthogonal projections for MMT detection and interference reduction," *IEEE Transactions on Geoscience and Remote Sensing*, vol. 52, no. 7, pp. 3800–3811, 2014.

[23] R. Bhalla and H. Ling, "A fast algorithm for simulating Doppler spectra of targets with rotating parts using the shooting and bouncing ray technique," *IEEE Transactions on Antennas and Propagation*, vol. 46, no. 9, pp. 1389–1391, 1998.

[24] G. Manfredi, I. D. S. Hinostroza, M. Menelle, S. Saillant, J.-P. Ovarlez, and L. Thirion-Lefevre, "Measurements and analysis of the doppler signature of a human moving within the forest in UHF-band," *Remote Sensing*, vol. 13, no. 3, 2021. [Online]. Available: https://www.mdpi.com/2072-4292/13/3/423

[25] G. Manfredi, J.-P. Ovarlez, and L. Thirion-Lefevre, "Features extraction of the Doppler frequency signature of a human walking at 1 GHz," in *IGARSS 2019 - 2019 IEEE International Geoscience and Remote Sensing Symposium*, 2019, pp. 2260–2263.

[26] "CST software," https://www.3ds.com/fr/produits-et-services/simulia/produits/cst-studio-suite.

[27] O. Bucci and G. Franceschetti, "On the spatial bandwidth of scattered fields," *IEEE Transactions on Antennas and Propagation*, vol. 35, no. 12, pp. 1445–1455, 1987.

[28] D. S. Ahmed, G. Cerri, P. Russo, L. Thirion-Lefèvre, R. Guinvarc'h, and G. Manfredi, "Efficient computation method for the electromagnetic scattering of complex targets," in *2021 XXXIVth General Assembly and Scientific Symposium of the International Union of Radio Science (URSI GASS)*, 2021, pp. 1–4.

[29] N. J. Willis, *Bistatic radar*, 2nd ed. SciTech Publishing, 2005. [Online]. Available: libgen.li/file.php?md5=ad9e601e1a929e15be813b085c801ced

[30] G. Manfredi, I. D. S. Hinostroza, M. Menelle, S. Saillant, J.-P. Ovarlez, and L. Thirion-Lefevre, "Measurements and analysis of the doppler signature of a human moving within the forest in uhf-band," *Remote Sensing*, vol. 13, no. 3, 2021. [Online]. Available: https://www.mdpi.com/2072-4292/13/3/423